PAPER

Check for updates

Fine structure in the solution state ^{13}C-NMR spectrum of C$_{60}$ and its endofullerene derivatives†

George Razvan Bacanu,* Gabriela Hoffman, Michael Amponsah, Maria Concistrè, Richard J. Whitby [ID] and Malcolm H. Levitt [ID]

The ^{13}C NMR spectrum of fullerene C$_{60}$ in solution displays two small "side peaks" on the shielding side of the main ^{13}C peak, with integrated intensities of 1.63% and 0.81% of the main peak. The two side peaks are shifted by −12.6 ppb and −20.0 ppb with respect to the main peak. The side peaks are also observed in the ^{13}C NMR spectra of endofullerenes, but with slightly different shifts relative to the main peak. We ascribe the small additional peaks to minor isotopomers of C$_{60}$ containing two adjacent ^{13}C nuclei. The shifts of the additional peaks are due to a secondary isotope shift of the ^{13}C resonance caused by the substitution of a ^{12}C neighbour by ^{13}C. Two peaks are observed since the C$_{60}$ structure contains two different classes of carbon–carbon bonds with different vibrational characteristics. The 2 : 1 ratio of the side peak intensities is consistent with the known structure of C$_{60}$. The origin and intensities of the ^{13}C side peaks are discussed, together with an analysis of the ^{13}C solution NMR spectrum of a ^{13}C-enriched sample of C$_{60}$, which displays a relatively broad ^{13}C NMR peak due to a statistical distribution of ^{13}C isotopes. The spectrum of ^{13}C-enriched C$_{60}$ is analyzed by a Monte Carlo simulation technique, using a theorem for the second moment of the NMR spectrum generated by J-coupled spin clusters.

1 Introduction

The ^{13}C solution NMR spectrum of C$_{60}$ fullerene is widely believed to contain a single peak. Indeed the observation of a single ^{13}C peak in the solution NMR of C$_{60}$ was one of the key pieces of evidence for its highly symmetrical structure.[1,2] All sixty ^{13}C sites are chemically equivalent and have an identical chemical shift, as opposed to less symmetrical fullerenes such as C$_{70}$ which displays 5 peaks in the ^{13}C spectrum.[1]

Nevertheless, close examination of the high resolution ^{13}C spectrum of C$_{60}$ in solution reveals two small additional peaks at a slightly lower chemical shift with respect to the main peak, in an intensity ratio of 2 : 1 (Fig. 1). Pairs of side peaks are also observed in the ^{13}C solution NMR spectrum of endofullerenes, in which the C$_{60}$ cages encapsulate guest molecules such as H$_2$ and H$_2$O (Fig. 2). The ^{13}C chemical shifts of the fullerene cage sites are perturbed by the endohedral guests within the cavity of C$_{60}$, leading to two main peaks (for empty and filled fullerene molecules) and two pairs of small side peaks, each with an amplitude ratio of 2 : 1.
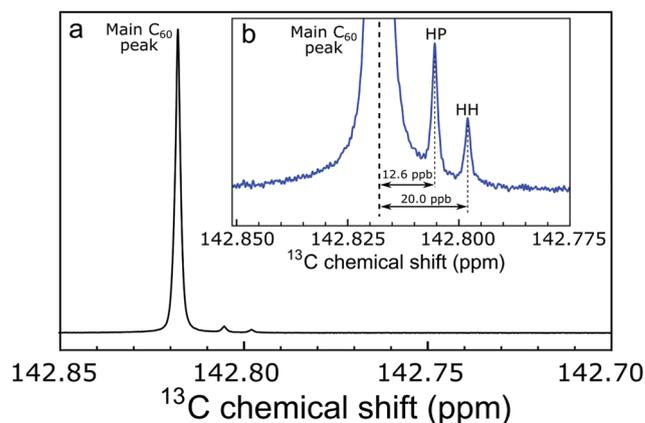

Fig. 1 (a) ^{13}C NMR spectrum of 25 mM C$_{60}$ in deuterated orthodichlorobenzene (ODCB-d$_4$), at a magnetic field of 16.45 T and a temperature of 295 K (sum of 856 transients). The main C$_{60}$ peak is at 142.818 ppm relative to TMS. (b) Expanded view of the base of the main C$_{60}$ peak, showing the assignment of the side peaks to ^{13}C pairs sharing either a HP (hexagon–pentagon) or a HH (hexagon–hexagon) bond. The secondary ^{13}C isotope shifts are $^1\Delta \simeq 12.6$ ppb for a HP ^{13}C$_2$ pair and $^1\Delta \simeq 20.0$ ppb for a HH ^{13}C$_2$ pair.

The pairs of side peaks may be attributed to minor isotopomers of C$_{60}$ with two ^{13}C nuclei in neighbouring carbon sites. The substitution of the abundant ^{12}C isotope at a particular site by the heavier ^{13}C isotope leads to secondary isotope shifts in the resonance frequencies of neighbouring ^{13}C sites.[3–8]

Departament of Chemistry, University of Southmapton, Southampton SO17 1BJ, UK. E-mail: g.r.bacanu@soton.ac.uk, mhl@soton.ac.uk; Tel: +44 (0)23 80596753

† Electronic supplementary information (ESI) available: Fitting procedure, spin–lattice relaxation, chemical shift referencing, mass spectrometry. See DOI: 10.1039/d0cp01282c
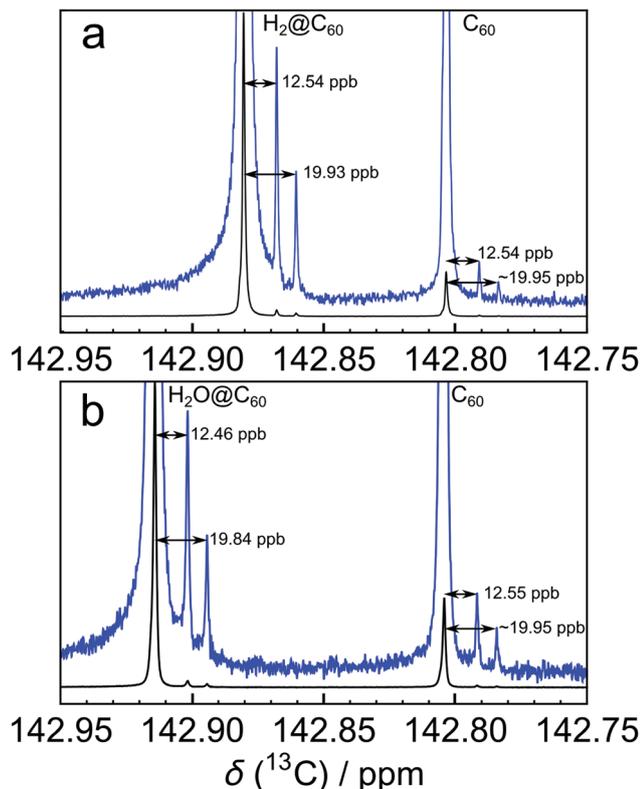
11850 | *Phys. Chem. Chem. Phys.*, 2020, **22**, 11850–11860

This journal is © the Owner Societies 2020

Fig. 2 ^{13}C NMR spectra of ~25 mM solutions of (a) $H_2@C_{60}$ (filling factor 87.7%, sum of 416 transients) and (b) $H_2O@C_{60}$ (filling factor 78.6%, sum of 272 transients) in ODCB-d_4 at a temperature of 298 K. For each species, a pair of side peaks on the shielding side of the main ^{13}C peak is clearly visible.

This shift arises since the vibrational wavefunctions of the participating nuclei are perturbed by the introduction of a nuclide with an increased mass. Since the structure of C_{60} contains two different classes of carbon–carbon bond with different vibrational characteristics, the ^{13}C spectrum of C_{60} and its derivatives contains two side peaks. As discussed below, the 2:1 intensity ratio of the two side peaks reflects the relative abundance of the C–C bond types in C_{60}. Note that the side peak structure is not caused by ^{13}C–^{13}C J-couplings, since the two ^{13}C nuclei in $^{13}C_2$ isotopomers of C_{60} are magnetically equivalent.

The aim of this paper is to provide an interpretation of the observed spectral structure in the ^{13}C NMR of C_{60} fullerene and its endofullerene derivates. The ^{13}C NMR spectrum of ^{13}C-enriched C_{60} is also presented, and analyzed using an approximate Monte Carlo simulation method exploiting a theorem for the second moment of the NMR spectra of J-coupled spin clusters.

2 Methods

Fullerene C_{60} was purchased from Materials Technologies Research Ltd (Cleveland, Ohio, USA) and purified by sublimation in-house. A solution was prepared by dissolving 23.4 mg of sublimed C_{60} powder in ~1.1 mL of *ortho*-dichlorobenzene-d_4

(ODCB-d_4, Sigma-Aldrich), adding ~10 μL of tetramethylsilane (TMS) for chemical shift referencing and ~100 μL of tris(trimethyl-silyl)silane for temperature calibration.[9] The solution was filtered to remove any undissolved impurities and degassed by bubbling O_2-free N_2 gas through the solution for 10 min.

The endofullerenes $H_2@C_{60}$ and $H_2O@C_{60}$ were prepared by molecular surgery techniques.[10–14] Fig. 2(a) shows the ^{13}C NMR spectrum of $H_2@C_{60}$ in ODCB-d_4, with a "filling factor" (*i.e.* fraction of filled cages) of 87.7%. The solution of $H_2O@C_{60}$ in ODCB-d_4 used for Fig. 2(b) contained $H_2O@C_{60}$ with a filling factor of 78.6%.

The ^{13}C-enriched fullerene was purchased as 20–30% ^{13}C-enriched powder from MER Corporation (Tucson, Arizona, USA) and sublimed in-house. 15.5 mg of sublimed powder was dissolved in 1 mL of ODCB-d_4 plus ~10 μL of TMS. The solution was filtered to remove undissolved impurities and degassed by O_2-free N_2 bubbling for 10 min.

All NMR experiments were performed at a field of 16.45 T in a Bruker Ascend 700 NB magnet fitted with a Bruker TCI prodigy 5 mm liquids cryoprobe and a Bruker AVANCE NEO console.

3 Results

The ^{13}C solution NMR spectrum of C_{60} is shown in Fig. 1. The two side peaks are at $\Delta\delta_1 = -12.6$ ppb and $\Delta\delta_2 = -20.0$ ppb relative to the main ^{13}C peak. In all measurements presented the widths of peaks (main and side peaks) at half-maximum height are between 0.128 Hz and 0.272 Hz, the bulk of measurements having line widths under 0.200 Hz. The integrated amplitudes of the side peaks, relative to the main ^{13}C peak, are $a_1/a_0 = 1.63 \pm 0.15\%$ and $a_2/a_0 = 0.81 \pm 0.08\%$ respectively (see the ESI† for the fitting procedure). The ratio of the integrated amplitudes for the two side peaks is given by $a_1/a_2 = 2.02 \pm 0.01$. Solutions of endofullerenes display an identical fine structure in their ^{13}C NMR peaks, as shown in Fig. 2.

The shifts of the side peaks relative to the main peak have a weak temperature-dependence, as shown in Fig. 3. The temperature-dependent shifts fit well to a linear model over the explored temperature range, of the form $\Delta\delta_i = \Delta\delta_i^0 + (d\Delta\delta_i/dT)T$ with $i \in \{1,2\}$. The fit parameters for C_{60} and two endofullerenes are given in Table 1. The outer side peak has a stronger temperature dependence than the inner peak and is slightly more affected by the presence of an endohedral molecule.

Enrichment of C_{60} with ^{13}C obscures the side peak structure. A ^{13}C NMR spectrum of a solution of 20–30% ^{13}C-enriched C_{60} in ODCB-d_4 is shown in Fig. 4(b). Instead of two discrete side peaks, a relatively broad lineshape is observed with a width of about 40 ppb. The broad peak exhibits a distinct shoulder on the deshielding ("downfield") side of the peak, at a chemical shift corresponding to the main ^{13}C peak in natural-abundance C_{60} (see ESI† for chemical shift referencing).

The ^{13}C relaxation time constants T_1 were also measured (see ESI†). The ^{13}C T_1 of the natural-abundance C_{60} sample was determined to be 16.6 ± 0.3 s at a temperature of 295 K and magnetic field of 16.45 T. The ^{13}C T_1 of the 20–30%
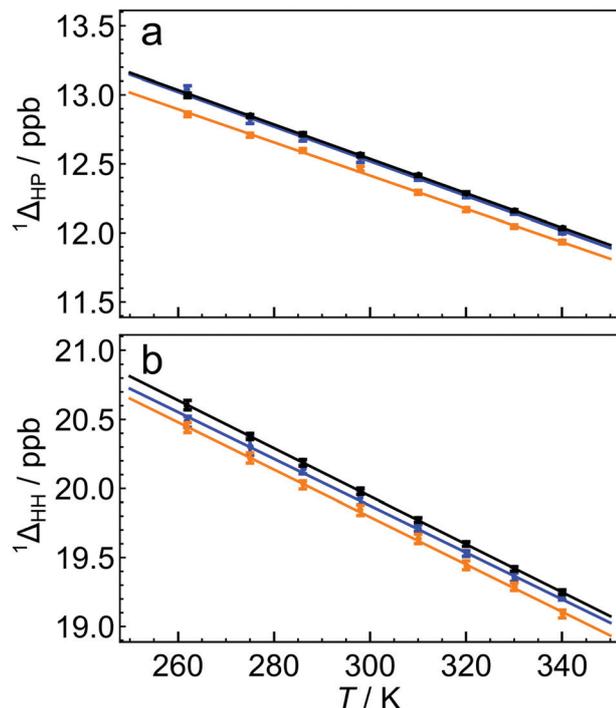
This journal is © the Owner Societies 2020

Phys. Chem. Chem. Phys., 2020, **22**, 11850–11860 | **11851**

Fig. 3 Temperature dependence of secondary ^{13}C isotope shifts for C$_{60}$ (black), H$_2$@C$_{60}$ (blue) and H$_2$O@C$_{60}$ (orange), for (a) HP the first side peak, and (b) HH the second side peak. The solid lines are best linear fits of the form $^1\Delta(T) = {}^1\Delta^0 + (\mathrm{d}^1\Delta/\mathrm{d}T)T$, where the fit parameters are given in Table 1. The side peak shifts $\Delta\delta_1$ and $\Delta\delta_2$ are related to the isotope shifts by a sign change (see eqn (3)).

^{13}C-enriched sample was found to be slightly shorter under the same conditions (14.8 ± 0.2 s).

4 Discussion

4.1 Natural abundance spectra

The molecular structure of C$_{60}$ is composed of sixty carbon atoms at the vertices of a truncated icosahedron (see Fig. 5). The carbon atoms are arranged in 20 hexagonal and 12 pentagonal rings. There are two distinct types of carbon–carbon bonds, with different bond lengths.[15–18] There are 30 carbon–carbon bonds which are on the shared edges of two hexagons, and which are called here HH bonds.[19,20] The HH bonds are significantly shorter than the 60 bonds which are shared between a hexagon and a pentagon, and which are called here HP bonds.[19,20]
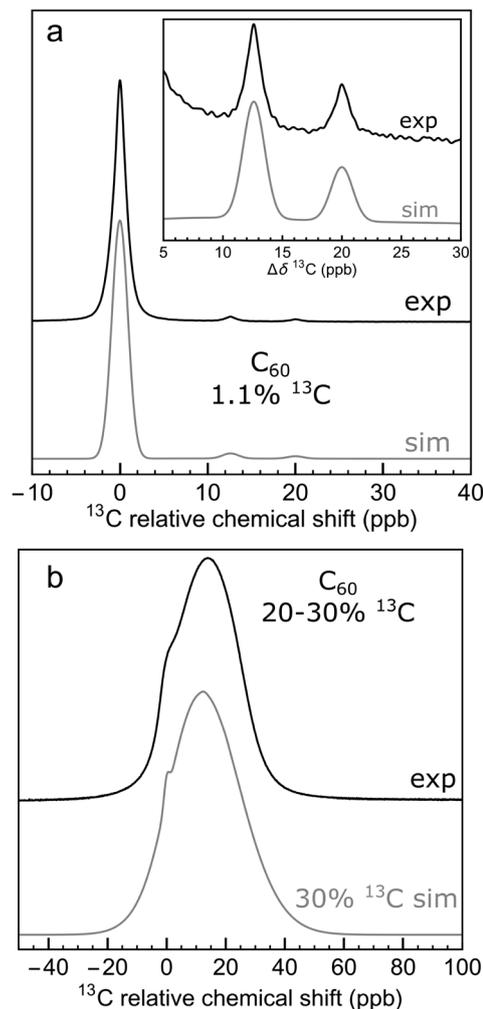

Fig. 4 (a) ^{13}C NMR spectrum of 25 mM solution of C$_{60}$ in ODCB-d$_4$ (sum of 856 transients); (b) ^{13}C NMR spectrum of 20 mM of ^{13}C-enriched C$_{60}$ (20–30% ^{13}C) in ODCB-d$_4$ (sum of 16 transients). Spectra are taken at 16.45 T and 295 K. Black lines show experimental data. The grey lines show the results of Monte Carlo simulations using a ^{13}C abundance of (a) 1.1% and (b) 30%. The horizontal axes depict the ^{13}C chemical shift relative to that of the main C$_{60}$ peak.

The internuclear distances for the two bond types are estimated to be r_{HH} = 139.5 ± 0.5 pm and r_{HP} = 145.2 ± 0.2 pm, as determined by X-ray diffraction,[15] gas-phase electron diffraction,[16] solid-state NMR,[17] and neutron diffraction.[18]

Table 1 Linear regression parameters for the temperature dependence of the secondary ^{13}C isotope shifts for C$_{60}$ and the endofullerenes H$_2$@C$_{60}$ and H$_2$O@C$_{60}$ (Fig. 3). The side peak shifts $\Delta\delta_1$ and $\Delta\delta_2$ are related to the isotope shifts by a sign change (see eqn (3))

Parameter	C$_{60}$	H$_2$@C$_{60}$	H$_2$O@C$_{60}$
$^1\Delta_{HP}$(298 K)/ppb	12.56 ± 0.01	12.54 ± 0.03	12.46 ± 0.02
$^1\Delta^0_{HP}$/ppb	16.28 ± 0.05	16.29 ± 0.11	16.03 ± 0.06
$(\mathrm{d}^1\Delta_{HP}/\mathrm{d}T)/10^{-3}$ ppb K^{-1}	−12.47 ± 0.15	−12.56 ± 0.34	−12.04 ± 0.20
$^1\Delta_{HH}$(298 K)/ppb	19.98 ± 0.02	19.93 ± 0.05	19.84 ± 0.04
$^1\Delta^0_{HH}$/ppb	25.16 ± 0.10	24.96 ± 0.18	24.94 ± 0.14
$(\mathrm{d}^1\Delta_{HH}/\mathrm{d}T)/10^{-3}$ ppb K^{-1}	−17.38 ± 0.30	−16.96 ± 0.58	−17.17 ± 0.44

11852 | Phys. Chem. Chem. Phys., 2020, 22, 11850–11860

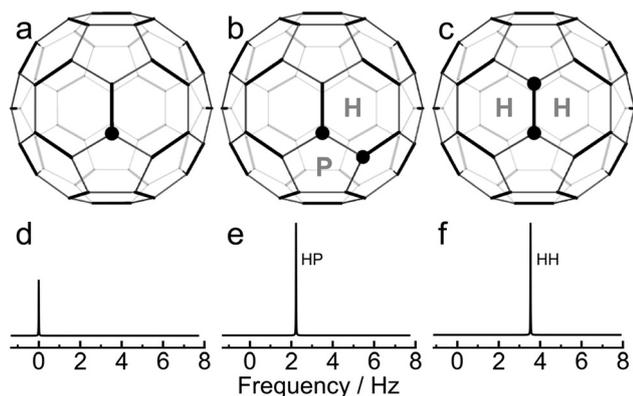This journal is © the Owner Societies 2020

Fig. 5 Three isotopomers of C_{60}, with the positions of ^{13}C sites marked by a filled circle: (a) $[^{13}C_1]$-C_{60}; (b) $[HP$-$^{13}C_2]$-C_{60}; (c) $[HH$-$^{13}C_2]$-C_{60}. The hexagonal and pentagonal carbon rings are marked. (d–f) Simulations of the associated ^{13}C spectra at a magnetic field of 16.45 T, using artificial Lorentzian lineshapes and secondary isotope shifts taken from experiment (Fig. 1). The spectral amplitudes contributed by each $^{13}C_2$ molecule is twice as large as for each $^{13}C_1$ molecule. The ^{13}C–^{13}C J-coupling does not influence the spectra of the $^{13}C_2$ isotopomers, since the ^{13}C nuclei are in magnetically equivalent sites.

The structure of C_{60} provides a ready qualitative interpretation of the natural abundance ^{13}C spectrum. The three species contributing most of the intensity to the natural abundance ^{13}C spectrum are denoted $[^{13}C_1]$-C_{60}, $[HP$-$^{13}C_2]$-C_{60}, and $[HH$-$^{13}C_2]$-C_{60} (see Fig. 5). $[^{13}C_1]$-C_{60} molecules contain ^{13}C sites with no immediate ^{13}C neighbours, while $[HP$-$^{13}C_2]$ $-C_{60}$ and $[HH$-$^{13}C_2]$-C_{60} molecules contain $^{13}C_2$ pairs separated by a HP bond and a HH bond respectively. On average, there are twice as many $[HP$-$^{13}C_2]$-C_{60} molecules as $[HH$-$^{13}C_2]$-C_{60} molecules, since there are twice as many HP bonds as HH bonds.

The $[^{13}C_1]$-C_{60} isotopomer contributes a single ^{13}C peak to the ^{13}C spectrum, at the main peak chemical shift (Fig. 5d). The $^{13}C_2$ pairs in the $[HP$-$^{13}C_2]$-C_{60} and $[HH$-$^{13}C_2]$-C_{60} isotopomers also contribute a single peak each (see Fig. 5e and f), since the ^{13}C sites are magnetically equivalent by symmetry. The ^{13}C–^{13}C J-coupling between magnetically equivalent spins has no direct spectral consequences in isotropic solution.[21] The spectral contribution from each $[HP$-$^{13}C_2]$-C_{60} and $[HH$-$^{13}C_2]$-C_{60} molecule is twice as large as the contribution from each $[^{13}C_1]$-C_{60} molecule.

The frequencies of the $[HP$-$^{13}C_2]$-C_{60} and $[HH$-$^{13}C_2]$-C_{60} peaks are influenced by secondary isotope shifts. The substitution of a ^{12}C nucleus by a more massive ^{13}C nucleus modifies the vibrational wavefunctions of the molecule and influences the chemical shift of neighbouring ^{13}C nuclei. The primary mechanism of secondary isotope shifts is as follows:[3–7] The chemical shift of a nucleus depends on the molecular electronic wavefunction which is a function of internuclear distances; the distances between bonded atoms oscillate because of vibrational motions and, within the Born–Oppenheimer approximation, the electronic wavefunction adjusts rapidly to the changing positions of the nuclei. The observed chemical shift is an average over the internuclear distances explored by the nuclear vibrational wavefunction. However, nuclear vibrational wavefunctions depend on the nuclear mass; heavier nuclei possess wavefunctions which are more strongly localised towards the potential minimum of the vibrational coordinate whereas lighter nuclei explore a wider range of vibrational coordinates. If the vibration is anharmonic, the mean nuclear position also depends on the nuclear mass. Hence, one-bond isotope shifts depend on the frequency and anharmonicity of the relevant vibrational mode. Since the two types of bonds in C_{60} have different bond lengths and vibrational frequencies, it is not surprising that the associated isotope shifts are different as well. The experimental results indicate that the secondary isotope shift is larger for two ^{13}C nuclei separated by the shorter HH bond, than when the nuclei are separated by the longer HP bond.

Unfortunately, the most widely used definition of the secondary isotope shift[6] suffers from a counter-intuitive sign convention. Nevertheless, we persist with it in this article. The secondary isotope shift of a ^{13}C site induced by swapping the "light" isotope ^LA of a neighbouring atom A with a "heavy" isotope ^HA is defined as follows:[6]

$$^1\Delta^{13}C\,(A) = \delta^{13}C\,(^LA) - \delta^{13}C\,(^HA) \tag{1}$$

The following condensed notation is introduced for the one-bond secondary isotope shifts in fullerenes:

$$^1\Delta_{HP} = \delta^{13}C\,([^{13}C_1]\text{-}C_{60}) - \delta^{13}C\,([HP\text{-}^{13}C_2]\text{-}C_{60})$$

$$^1\Delta_{HH} = \delta^{13}C\,([^{13}C_1]\text{-}C_{60}) - \delta^{13}C\,([HH\text{-}^{13}C_2]\text{-}C_{60}) \tag{2}$$

The chemical shifts of the two side peaks, relative to the main ^{13}C peaks, are therefore given by

$$\Delta\delta_1 = -^1\Delta_{HP}$$

$$\Delta\delta_2 = -^1\Delta_{HH} \tag{3}$$

The HP and HH peak assignments are shown in Fig. 1 and 5. The amplitudes of the two side peaks are in the ratio $2:1$ since C_{60} contains twice as many HP bonds as HH bonds. This is in agreement with experiment.

The interpretation of the natural-abundance ^{13}C spectrum of C_{60} therefore appears to be straightforward. The main ^{13}C peak derives from $^{13}C_1$ isotopomers of C_{60}, while the two side peaks derive from the two types of $^{13}C_2$ isotopomers, which have abundances in the ratio of $2:1$. However, closer inspection reveals one small point that is not so easy to explain. The ratio of the integrated amplitude of the outer (HH) side peak to that of the main peak is observed to be $a_2/a_0 = 0.81 \pm 0.08\%$. What explains this intensity ratio? A naive theory runs as follows: The outer side peak is attributed solely to the $[HH$-$^{13}C_2]$-C_{60} iso-topomer, and the main peak to the $[^{13}C_1]$-C_{60} isotopomer. Consider two neighbouring carbon sites in C_{60}, separated by a HH bond. The probability of a carbon atom having a ^{13}C nucleus is x, while the probability of the carbon having a ^{12}C nucleus is $1 - x$. The probability of either one of the two sites being ^{13}C is therefore given by $2x(1 - x)$. Both $^{13}C_1$ isotopomers contribute to the intensity of the main ^{13}C peak. The probability of both sites being ^{13}C, on the other hand, is x^2. The ^{13}C resonance of these $^{13}C_2$ isotopomers is subject to the

This journal is © the Owner Societies 2020

Phys. Chem. Chem. Phys., 2020, **22**, 11850–11860 | **11853**

secondary isotope shift and hence they contribute to the intensity of the HH side peak. Since a $^{13}C_2$ isotopomer contributes twice the spectral intensity of a $^{13}C_1$ isotopomer, the amplitude ratio of the HH side peak to the main peak is predicted by this argument to be $2 \times x^2/2x(1 - x) = x/(1 - x)$. This is given approximately by x for small x. Since the natural abundance of ^{13}C is $x \simeq 1.1\%$, the predicted amplitude ratio is also 1.1%. However, this prediction is outside the confidence limits of the observed a_2/a_0 ratio, which is $0.81 \pm 0.08\%$. The discrepancy is significant.

As shown below, a more sophisticated theory of the spectral structure is required to explain the observed intensity ratio of the side peaks to the main peak. Alternative combinatorial approach is given in the ESI.†

Fig. 3 shows that the isotope shifts $^1\Delta_{HP}$ and $^1\Delta_{HH}$ decrease as the temperature is increased. This may be attributed to the increased representation of excited vibrational states as the temperature is increased; excited vibrational wavefunctions are less influenced by the mass of the vibrating particles than the ground vibrational state.[5] It is not fully understood why the HH bond exhibits a stronger temperature-dependence than the HP bond. This may be due to the fact that the HH bond is shorter than the HP bond and has a higher force constant. The vibrational excited states of the HH bond are therefore less accessible, causing an increase in temperature to have a proportionately higher effect on the populations of excited vibrational wavefunctions.

Fig. 3 and Table 1 show that the isotope shifts are slightly reduced in magnitude when an endohedral molecule is present. The larger the endohedral molecule, the larger the change in the isotope shift. The mechanism of this effect is currently unknown, but it may be associated with a modification of the C_{60} vibrational modes by the endohedral moiety, an effect which has been detected in Raman spectroscopy.[22]

4.2 ^{13}C-enriched fullerene and spectral simulations

The ^{13}C NMR spectrum of ^{13}C-enriched C_{60} is shown in Fig. 4(b) and displays a relatively broad lineshape with a shoulder on the deshielding side of the peak. The position of the shoulder coincides with the position of the main peak in natural abundance C_{60} (see ESI†).

There is a small difference in the spin–lattice relaxation rate constants of the natural-abundance and ^{13}C-enriched samples (see ESI†). This difference is presumably due to the role of ^{13}C–^{13}C dipole–dipole couplings. However, the small relaxation rate difference is insufficient to explain the spectral broadening in the ^{13}C spectrum of ^{13}C-enriched C_{60}. The broad lineshape originates from coherent interactions, such as secondary isotope shifts and ^{13}C–^{13}C J-couplings.

A detailed understanding of this spectral structure presents a formidable theoretical and computational challenge. At an enrichment level of 30%, the most abundant isotopomers of C_{60} contain around 19 ^{13}C nuclei.[25] An accurate simulation of even a single spin system of this size is at the very limit of current computational techniques. An accurate simulation would require the calculation of an astronomical number of such spectra, some of which involve much larger spin systems.

Nevertheless, the rather featureless lineshape in Fig. 4(b) indicates that a detailed lineshape analysis is unnecessary in this case. It is possible to achieve a reasonable qualitative understanding of the lineshape through a Monte Carlo technique aided by plausible approximations and assumptions.

The simulation technique involves the following steps: (i) generation of a computer representation of an ensemble of ^{13}C configurations, distributed according to the desired ^{13}C abundance; (ii) identification of one or more distinct ^{13}C clusters within each configuration; (iii) prediction of spin interaction parameters (chemical shifts and J-couplings) for each ^{13}C cluster; (iv) calculation of the spectral lineshape for an individual ^{13}C cluster with the predicted interaction parameters; (v) summation of the simulated lineshapes over all ^{13}C clusters, leading to the total NMR spectrum:

$$S(\omega) = N_{\text{config}}^{-1} \sum_{c=1}^{M} S_c(\omega) \qquad (4)$$

Here $S_c(\omega)$ is the simulated NMR spectrum for an individual cluster, M is the number of clusters and the total number of configurations is denoted N_{config}.

The details of the individual steps are as follows:

(1) Generation of an ensemble of ^{13}C configurations. The atomic coordinates and bonding network for C_{60} are set up in the Mathematica symbolic software platform.[26] A ^{13}C or ^{12}C nucleus is randomly assigned to each of the 60 carbon sites using a stochastic function with probability x for ^{13}C and $1 - x$ for ^{12}C. Typical calculations involve around $N_{\text{config}} = 10\,000$ random configurations. This is far smaller than the total number of possible configurations but sufficient to define the main features of the NMR spectrum.

(2) Identification of ^{13}C clusters. The next step is to identify ^{13}C clusters within each computer-generated configuration, by which we mean groups of ^{13}C spins which interact sufficiently strongly with each other to be treated as distinct spin systems, while interactions between spins in different clusters are ignored. Quantum chemistry calculations on C_{60} have predicted that the J_{CC} coupling between all pairs of ^{13}C nuclei separated by more than 3 bonds are smaller than 1 Hz.[23,24] Since 1 Hz corresponds to $\sim$6 ppb for ^{13}C in a magnetic field of 16.45 T, which is smaller in magnitude than the one-bond secondary isotope shifts, we define a ^{13}C cluster as follows: a set of ^{13}C nuclei for which (i) each nucleus is connected to at least one other member of the cluster by no more than 3 bonds, and (ii) for which every nucleus is at least 4 bonds away from any ^{13}C nuclei which are outside the cluster. For example, the configurations sketched in Fig. 6(a) and (b) each contain one ^{13}C cluster (containing 3 and 4 ^{13}C nuclei respectively), while the configuration in Fig. 6(c) contains one cluster of 2 ^{13}C nuclei and a second cluster of 4 ^{13}C nuclei. Note that a cluster does not necessarily consist of ^{13}C atoms which are directly bonded to each other. The number of ^{13}C nuclei in an individual cluster c is denoted N_c.

11854 | *Phys. Chem. Chem. Phys.*, 2020, **22**, 11850–11860
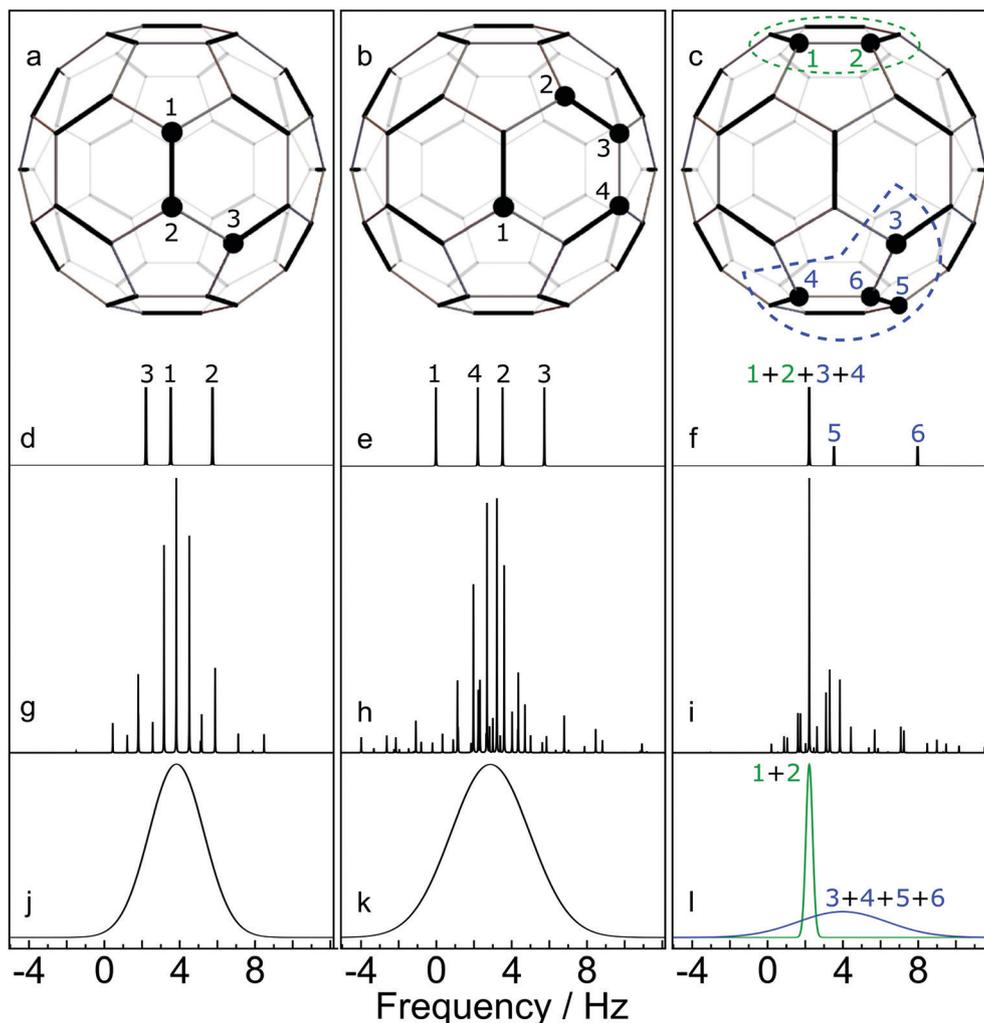
This journal is © the Owner Societies 2020

Fig. 6 Simulated NMR spectra for three selected C_{60} configurations, at a magnetic field of 16.45 T. ^{13}C nuclei are shown by filled circles. Cases (a) and (b) contain a single ^{13}C cluster. Case (c) contains two ^{13}C clusters. (d–f) Stick spectra showing the predicted ^{13}C chemical shifts, perturbed by the one-bond secondary isotope shifts from neighbouring ^{13}C nuclei; (g and h) Accurate spin dynamical computations of the NMR spectra, including the predicted chemical shifts and J-couplings from quantum chemistry calculations.[23,24] (i)–(l) Approximate simulations of the NMR spectra for each cluster using eqn (7). All vertical scales are arbitrary.

(3) Spin interaction parameters for a ^{13}C cluster. Simulation of the NMR spectrum of a ^{13}C cluster requires knowledge of the spin interaction parameters (chemical shifts and J-couplings). For the J-couplings between pairs of ^{13}C in the cluster we use the results of published quantum chemistry calculations.[24] For the chemical shifts, an additive model is assumed for the one-bond secondary isotope shifts. Suppose that a given ^{13}C site i has $n_{HP}(i)$ ^{13}C neighbours separated by a HP bond, where $n_{HP}(i) \in \{0,1,2\}$, and $n_{HH}(i)$ ^{13}C neighbours separated by a HH bond, where $n_{HH}(i) \in \{0,1\}$. The total secondary isotope shift of the given ^{13}C site is assumed to be given by

$$^{1}\Delta_i \simeq n_{HP}(i)^{1}\Delta_{HP} + n_{HH}(i)^{1}\Delta_{HH} \qquad (5)$$

where the values $^{1}\Delta_{HP}$ = 12.6 ppb and $^{1}\Delta_{HH}$ = 20.0 ppb are assumed in the calculations. All two-bond and higher secondary isotope shifts are ignored. The total secondary isotope shift has a maximum value of $2^{1}\Delta_{HP} + {}^{1}\Delta_{HH}$ = 45.2 ppb,

and a minimum value of 0. These two values approximately bound the lineshape of the ^{13}C-enriched sample of C_{60}, shown in Fig. 4(b).

The isotope shift of each ^{13}C site i may be converted into a frequency shift relative to the main ^{13}C peak by using the relationship

$$\Omega_i = -{}^{1}\Delta_i \times \omega^0 \qquad (6)$$

where the (signed) ^{13}C Larmor frequency is $\omega^0 = -\gamma B^0$, γ is the magnetogyric ratio of ^{13}C and B^0 is the magnetic field.[21] Eqn (6) takes into account the non-intuitive sign convention for the secondary isotope shift (eqn (3)).[6]

4. Spectral lineshape for a ^{13}C cluster. Having identified a ^{13}C cluster and estimated all chemical shifts and J-couplings, the next step is to simulate the ^{13}C spectrum.

In the case of small cluster dimension N_c, it is possible to use accurate simulation techniques, such as those used in the

SpinDynamica software package.[27] Some results are shown in the middle row of Fig. 6. In each case the simulations show a complex spectrum containing many individual peaks.

Accurate simulations of this type are not feasible for large values of N_c, and in any case this level of spectral detail is unresolved in the experimental spectra of ^{13}C-enriched C_{60}. We therefore use an approximate expression for the ^{13}C cluster spectrum $S_c(\omega)$, which derives from a moment analysis of the NMR spectrum, as described in the Appendix. The cluster spectrum is approximated by the following Gaussian function:

$$S_c^*(\omega) = N_c(2\pi\sigma_c)^{-1/2}\exp\left\{-\frac{(\omega - \bar{\Omega}_c)^2}{2\sigma_c}\right\} \qquad (7)$$

where the standard deviation of the Gaussian function is as follows:

$$\sigma_c = N_c^{-1}\sum_{i=1}^{N_c}\left(\Omega_i - \bar{\Omega}_c\right)^2 \qquad (8)$$

and the mean resonance offset frequency of a cluster is given by

$$\bar{\Omega}_c = N_c^{-1}\sum_{i=1}^{N_c}\Omega_i \qquad (9)$$

Eqn (7) evaluates very rapidly even for large cluster dimension N_c.

Fig. 6 compares some cluster spectra simulations using eqn (7) (lower row) with exact spin-dynamical simulations (middle row). The approximate method omits the fine details of the spectra but represents the centre frequency and width of the cluster spectra accurately. The great advantage of this approximation technique is that it is computationally feasible for large numbers of clusters each containing many ^{13}C nuclei, which is out of the question for accurate spin-dynamical techniques.

Eqn (8) predicts a zero-width Gaussian when all ^{13}C nuclei in the cluster have identical chemical shifts (magnetic equivalence). A small empirical line-broadening term is included in this case, matching the experimental linewidth of the natural-abundance C_{60} peak.

The ^{13}C NMR spectrum of C_{60} may therefore be treated approximately, for any ^{13}C probability x, by generating a large number of configurations using a Monte Carlo method, and summing the cluster contributions to the spectrum according to

$$S^*(\omega) = N_{\text{config}}^{-1}\sum_{c=1}^{M}S_c^*(\omega) \qquad (10)$$

where the individual spectral contributions are given by eqn (7).

Fig. 7(a) shows the result for $x = 1.1\%$, which corresponds to the incidence of ^{13}C at natural abundance. The two side peaks are just visible, and are seen more clearly in the expanded view
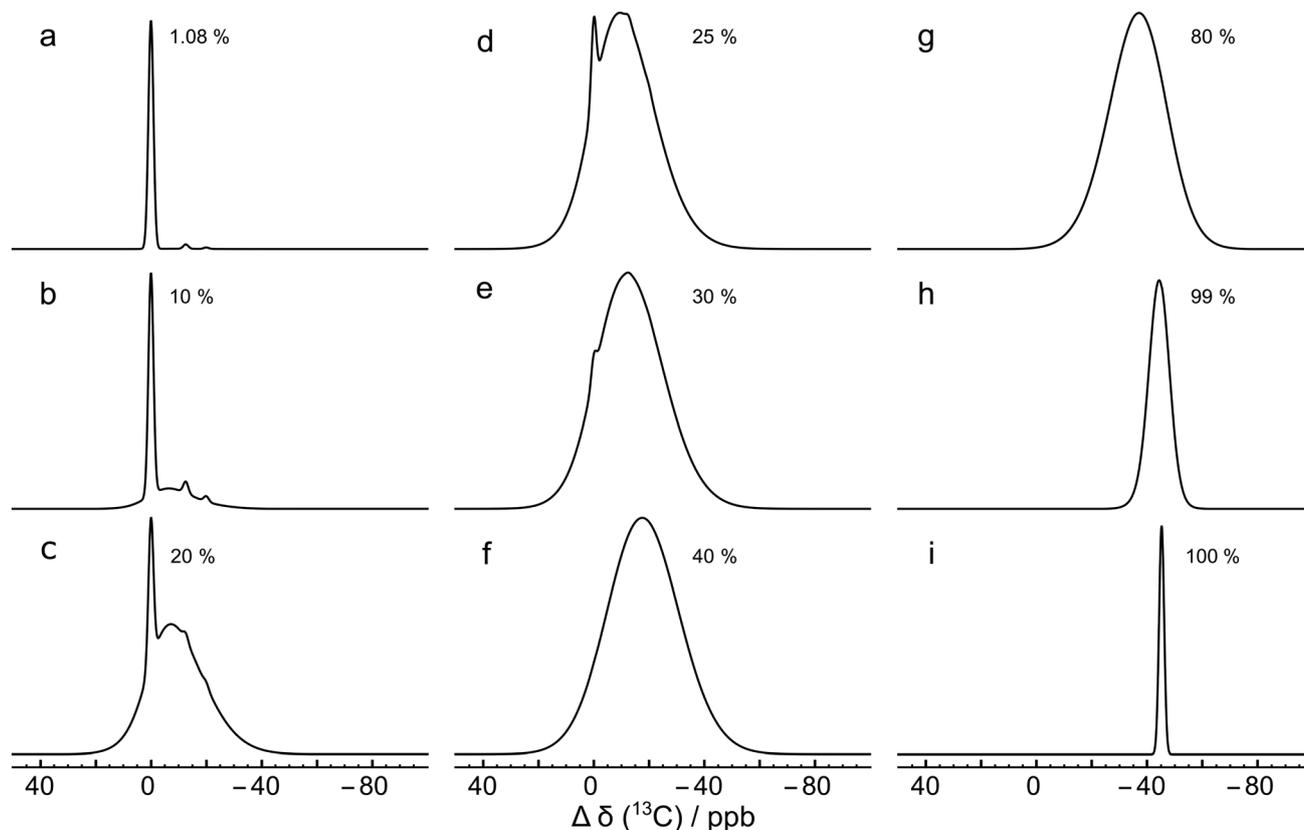

Fig. 7 Monte Carlo simulations of the ^{13}C NMR spectra of C_{60} with different values of the ^{13}C probability x, using eqn (10), at a magnetic field of $B^0 = 16.45$ T. Each simulation was performed by analyzing 10 000 random C_{60} configurations. The spectra are normalised to the same peak height for clarity. Simulations for more values of x are shown in the ESI.†

11856 | *Phys. Chem. Chem. Phys.*, 2020, **22**, 11850–11860

This journal is © the Owner Societies 2020

of Fig. 4(a), where the simulated and experimental spectra are compared. The correspondence is good.

Why is the ratio between the main ^{13}C peak and the second side peak not equal to $x \simeq 1.1\%$, as expected by a naive argument (see above)? The cluster analysis explains this by considering the role of the random ^{13}C occupancy of carbon sites which are 2 or 3 bonds away from the sites of interest. There are several ways to perform this analysis, all requiring care: the argument given below predicts the correct ratio using relatively few logical steps, but requires delicate reasoning. An alternative analysis is given the ESI,† this considers the relative abundances of C_{60} isotopomers containing up to three ^{13}C nuclei, and provides an estimate of the peak ratio which is close, but not exactly equal, to the experimental ratio. The residual discrepancy is attributed to isotopomers with more than three ^{13}C nuclei.

Consider the main ^{13}C peak. This derives predominantly from isolated ^{13}C nuclei. In the C_{60} structure, there are 3 carbon sites which are one bond away from a given site, 6 sites which are 2 bonds away, and 8 sites which are 3 bonds away. Assuming that a given carbon site is occupied by ^{13}C, there is a probability of $14x \simeq 15\%$ that at least one of the sites that are 2 or 3 bonds away are also occupied by ^{13}C. The two ^{13}C nuclei would, by the definition used in this article, belong to the same cluster. However, the spectral consequences of these additional ^{13}C nuclei are minor, since the additional nuclei will (most likely) not have direct one-bond ^{13}C neighbours themselves. Hence, the additional ^{13}C nucleus does not experience a significant secondary isotope shift, and the cluster of two ^{13}C nuclei has the same chemical shift as an isolated ^{13}C nucleus, within the approximations used here. The amplitude of the ^{13}C main peak is therefore largely unaffected by random pairs of ^{13}C nuclei which are 2 or 3 carbon–carbon bonds distant from each other.

The situation is different for the ^{13}C$_2$ pairs that give rise to the side peaks. A ^{13}C$_2$ pair separated by a HH bond has 4 carbon sites which are one bond away, 8 sites which are 2 bonds away, and 8 sites which are 3 bonds away. There is a probability of $16x \simeq 18\%$ that at least one of the sites that are 2 or 3 bonds away are also occupied by ^{13}C. Unlike the case of isolated ^{13}C nuclei, an additional ^{13}C nucleus 2 or 3 bonds away has a large effect on the spectrum. The three ^{13}C nuclei form a single cluster, which has a broadened and shifted spectrum, relative to the spectrum of the isolated ^{13}C$_2$ pair. This is because the additional ^{13}C nucleus does not itself have a directly-bonded neighbouring ^{13}C (except in rare circumstances), and therefore experiences a different secondary isotope shift to the directly-bonded ^{13}C$_2$ pair. Hence about 18% of the intensity of a given side peak is transferred into a broadened and shifted resonance. The result is a depletion in the intensity of the sharp side peak by $\sim$18%. This argument accounts accurately for the observed ratio in the relative intensities of the side peaks and the main peak in natural abundance C_{60}.

This effect is seen more clearly in Fig. 7(b), which shows a simulation for a ^{13}C probability of $x = 10\%$. The broad resonance between the main peaks and the side peaks is obvious in this case.

Fig. 7 shows that as the ^{13}C probability increases, the ^{13}C spectrum broadens and shifts in the shielding direction, with a shoulder at the main peak position persisting up to about $x = 30\%$. The shoulder is generated by ^{13}C nuclei that have no directly bonded ^{13}C partners themselves and which are also at least 3 bonds away from directly-bonded groups of ^{13}C nuclei. A simulation for $x = 30\%$ matches the experimental spectrum of the ^{13}C-enriched C_{60} well, as shown in Fig. 4(b). This is in agreement with the enrichment level determined by mass spectrometry, which is also $x \sim 30\%$ (see ESI†).

Fig. 7 shows that the simulated spectra become narrower again when x exceeds 50%. This is because the isotope shifts of the ^{13}C sites become more uniform when most carbon sites in C_{60} are occupied by ^{13}C. In the extreme case of $x = 100\%$, the simulated spectrum is very sharp, since all ^{13}C sites have three ^{13}C neighbours, and experience the same secondary isotope shift of $2^1\Delta_{HP} + {}^1\Delta_{HH} = 45.2$ ppb. All sixty ^{13}C nuclei are magnetically equivalent in this case.

5 Conclusion

The observation of a single, sharp ^{13}C NMR peak for solutions of C_{60} is one of the strongest pieces of evidence for its highly symmetrical molecular structure.[1] Our observations show that the solution-state ^{13}C NMR of C_{60} also displays two small side peaks, in the intensity ratio of 2:1. We interpret the side peaks as the signals from ^{13}C$_2$ isotopomers, which are displaced from the main ^{13}C peak by secondary isotope shifts. Two peaks arise since the C_{60} structure contains two types of carbon–carbon bonds, also in the incidence ratio of 2:1. Indeed the presence of two side peaks in the solution ^{13}C spectrum of C_{60} proves the presence of two different types of C–C bonds – a fact which was originally established by X-ray diffraction,[15] gas-phase electron diffraction,[16] neutron diffraction[18] and low-temperature solid-state NMR of ^{13}C labelled material.[17]

^{13}C side peaks of similar origin are also observed for other symmetrical molecular compounds, such as ferrocene.[28]

The secondary isotope shifts become smaller when the temperature is increased. The positions of the side peaks are also influenced by the presence of an endohedral molecule, with the magnitude of the perturbation roughly correlated with the size of the endohedral moiety.

The solution ^{13}C NMR spectrum of ^{13}C-enriched C_{60} is broader than that of the natural abundance material. We have developed an algorithm for the simulation of C_{60} NMR spectra at arbitrary levels of ^{13}C enrichment. This uses a Monte Carlo approach, combined with a cluster identification algorithm, and an approximate spectral treatment based on a second moment analysis. This technique allows rapid approximate calculations of the NMR spectra of J-coupled spin clusters, even for large numbers of coupled spins, and might be adapted to other problems in solution and solid-state NMR. The simulations agree well with the experimental spectrum of the ^{13}C-enriched sample. This analysis also explain why the outer side peak in natural-abundance C_{60} has an amplitude of 0.81%

This journal is © the Owner Societies 2020

Phys. Chem. Chem. Phys., 2020, 22, 11850–11860 | 11857

of the main peak, instead of the natural abundance ratio of 1.1%, which would be predicted by a naive argument.

We expect that the ^{13}C NMR spectra of higher fullerenes such as C_{70} will also display additional spectral structure due to $^{13}C_2$ isotopomers. In this case, more complex phenomena are anticipated since there are several groups of chemically inequivalent sites.

Conflicts of interest

There are no conflicts to declare.

Appendix

Approximate NMR spectrum of J-coupled spin clusters

Consider a cluster c containing N_c J-coupled spins-1/2, with chemical shifts δ_i and J-couplings J_{ij}, where $i, j \in \{1 \ldots N\}$. The rotating-frame spin Hamiltonian in isotropic solution is given by

$$H = H_{CS} + H_J \tag{11}$$

where the chemical shift and J-coupling terms are given by

$$H_{CS} = \sum_{i=1}^{N_c} \Omega_i I_{iz}; \quad H_J = \sum_{i<j}^{N_c} 2\pi J_{ij} \mathbf{I}_i \cdot \mathbf{I}_j \tag{12}$$

and the resonance offset frequencies by

$$\Omega_i = -\gamma B^0 (\delta_i - \delta_{ref}) \tag{13}$$

The Hamiltonian may be written as follows:

$$H = H_0 + H_1 \tag{14}$$

where H_0 is defined as follows:

$$H_0 = \bar{\Omega}_c I_z \tag{15}$$

and the mean offset frequency for the cluster is defined in eqn (9).

The term H_1 is given by

$$H_1 = H_J + \sum_{i=1}^{N_c} \Delta\Omega_i I_{iz} \tag{16}$$

where $\Delta\Omega_i$ are resonance offsets with respect to the mean cluster frequency:

$$\Delta\Omega_i = \Omega_i - \bar{\Omega}_c \tag{17}$$

The NMR signal for the cluster (free-induction decay) is given by

$$s_c(t) = (Q_{obs}|\exp(-i\hat{H}t)\rho(0)) \tag{18}$$

where $\hat{H}$ is the commutation superoperator of the Hamiltonian H, and the Liouville bracket is defined:[29]

$$(A|B) = \text{Tr}\{A^\dagger B\} \tag{19}$$

Since the Hamiltonian terms H_0 and H_1 commute, the cluster NMR signal may be written

$$s_c(t) = (Q_{obs}\exp(+i\hat{H}_0 t)|\exp(-i\hat{H}_1 t)\rho(0)) \tag{20}$$

The spin density operator at the start of signal detection is denoted $\rho(0)$ and the observable operator is denoted Q_{obs}. In an ordinary single-pulse NMR experiment, using quadrature detection, it is convenient to define these operators as follows:[21]

$$\rho(0) = -I_y$$
$$Q_{obs} = -iI^- \tag{21}$$

With this choice of observable operator the following commutation relationship holds:

$$\hat{H}_0|Q_{obs}) = -\bar{\Omega}_c|Q_{obs}) \tag{22}$$

and hence

$$\exp(-i\hat{H}_1 t)|Q_{obs}) = \exp(+i\bar{\Omega}_c t)|Q_{obs}) \tag{23}$$

This leads to the following expression for the cluster NMR signal:

$$s_c(t) = g_c(t)\exp(i\bar{\Omega}_c t) \tag{24}$$

where the function $g_c(t)$ is defined as follows:

$$g_c(t) = (Q_{obs}|\exp(-i\hat{H}_1 t)\rho(0)) \tag{25}$$

The NMR spectrum of the cluster is given by the one-sided Fourier transform of the NMR signal:

$$S_c(\omega) = \int_0^\infty s_c(t)\exp(-i\omega t)dt \tag{26}$$

which may be written as follows:

$$S_c(\omega) = G_c(\omega - \bar{\Omega}_c) \tag{27}$$

where the function $G_c(\omega)$ is the Fourier transform of $g_c(t)$:

$$G_c(\omega) = \int_0^\infty g_c(t)\exp(-i\omega t)dt \tag{28}$$

Eqn (27) shows that the cluster spectrum $S_c(\omega)$ may be derived from the function $G_c(\omega)$ by a simple frequency shift. The function $G_c(\omega)$ is centred around $\omega = 0$, while the spectrum $S_c(\omega)$ is centered around the mean resonance offset $\bar{\Omega}_c$.

An approximate expression for $G_c(\omega)$ is developed by a moment analysis. The use of spectral moments is known to be a powerful technique in broad-line solid-state NMR,[30] but has rarely been used for solution NMR. The nth moment $M_c^{(n)}$ of the real part of the function $G_c(\omega)$ is defined as follows:

$$M_c^{(n)} = \int_{-\infty}^\infty \text{Re}\{G_c(\omega)\}\omega^n d\omega \tag{29}$$

From the properties of the Fourier transform,[31] the nth moment of the real part of the spectrum is proportional to

the nth derivative of the time-domain signal at the time origin:

$$M_c^{(n)} = (-i)^n \left(\frac{d^n}{dt^n} g_c(t) \right)_{t=0} \tag{30}$$

Repeated differentiation of eqn (25) leads to the expression

$$\frac{d^n}{dt^n} g_c(t) = (-i)^n \left(Q_{obs} | \hat{H}_1^n \rho(t) \right) \tag{31}$$

and hence a compact form for the nth spectral moment of $G_c(\omega)$:

$$M_c^{(n)} = -i(-1)^n (\Gamma | \hat{H}_1^n I_y) \tag{32}$$

For example, the $n = 0$ moment, which is equal to the integral of the spectrum, evaluates to:

$$M_c^{(0)} = -i(+i)(I_y | I_y) = N_c 2^{N_c - 2} \tag{33}$$

using eqn (25).

The expression for the first moment of $G_c(\omega)$ involves the following terms:

$$\hat{H}_1 | I_y) = \hat{H}_J | I_y) + \sum_{i=1}^{N_c} \Delta\Omega_i \hat{I}_{iz} | I_y) \tag{34}$$

The first term vanishes since the J-coupling Hamiltonian commutes with the total angular momentum operator along an arbitrary axis:

$$[\mathbf{I}_i \cdot \mathbf{I}_j, I_{iy} + I_{jy}] = 0 \tag{35}$$

The commutation properties of the angular momentum operators lead to the following expression for the second term:

$$\hat{H}_1 | I_y) = \sum_{i=1}^{N_c} \Delta\Omega_i \hat{I}_{iz} | I_y) = -i \sum_{i=1}^{N_c} \Delta\Omega_i | I_{ix}) \tag{36}$$

Hence the first spectral moment is given by

$$M_c^{(1)} = \sum_{i=1}^{N_c} \Delta\Omega_i (\Gamma^- | I_{ix}) = 0 \tag{37}$$

The first moment of $G_c(\omega)$ vanishes since each bracketed term is identical, and the sum of the resonance offsets, relative to the mean frequency of the cluster, is zero by definition:

$$\sum_{i=1}^{N_c} \Delta\Omega_i = 0 \tag{38}$$

The second moment is conveniently evaluated by rearranging eqn (32) for $n = 2$:

$$M_c^{(2)} = -i(\Gamma^- \hat{H}_1 | \hat{H}_1 I_y) \tag{39}$$

All terms involving the J-coupling term H_J vanish through the commutation relationship in eqn (35). This leads through eqn (36) to the expression

$$M_c^{(2)} = \sum_{i,j=1}^{N_c} \Delta\Omega_i \Delta\Omega_j (I_{ix} | I_{jx}) \tag{40}$$

Since the angular momentum operators of different spins are orthogonal, we get

$$M_c^{(2)} = 2^{N_c - 2} \sum_{i=1}^{N_c} \Delta\Omega_i^2 \tag{41}$$

The normalized second moment, defined as the ratio of the second and zeroth moments, is given by

$$\mathcal{M}_c^{(2)} = \frac{M_c^{(2)}}{M_c^{(0)}} = N_c^{-1} \sum_{i=1}^{N_c} \Delta\Omega_i^2 \tag{42}$$

which is equal to the mean-sum-square of the resonance offsets for all spins in the cluster, relative to the mean resonance offset.

Note that the J-couplings do not appear in the expression for the second moment. The second moment of the NMR spectrum of a given J-coupled spin cluster may therefore be calculated extremely rapidly using only the chemical shift values for all spins in the cluster. The situation is different for the case of dipole–dipole coupled solids,[30] since a commutation relationship of the type given in eqn (35) does not apply for the dipole–dipole Hamiltonian.

The algorithm used in this paper uses the following Gaussian function as an approximation to the function $G_c(\omega)$:

$$G_c^*(\omega) = N_c \left(2\pi \mathcal{M}_c^{(2)} \right)^{-1/2} \exp \left\{ -\frac{\omega^2}{2\mathcal{M}_c^{(2)}} \right\} \tag{43}$$

where the normalized second moment is given by eqn (42). This expression omits the fine details of the NMR spectrum but has correct values for the zeroth, first, and second moments. The approximate form of the spectral function $S_c(\omega)$ for a cluster of ^{13}C spins, given in eqn (7), is derived from eqn (43) by using the expression for the second moment in eqn (42), and the frequency–shift relationship in eqn (27).

Acknowledgements

References

1 R. Taylor, J. P. Hare, A. K. Abdul-Sada and H. W. Kroto, *J. Chem. Soc., Chem. Commun.*, 1990, 1423–1425.

2 H. W. Kroto, A. W. Allaf and S. P. Balm, *Chem. Rev.*, 1991, **91**, 1213–1235.

3 H. Batiz-Hernandez and R. A. Bernheim, *Prog. Nucl. Magn. Reson. Spectrosc.*, 1967, **3**, 63–85.

4 W. T. Raynes, A. M. Davies and D. B. Cook, *Mol. Phys.*, 1971, **21**, 123–133.

5 C. J. Jameson, *J. Chem. Phys.*, 1977, **66**, 4983–4988.

6 P. E. Hansen, *Prog. Nucl. Magn. Reson. Spectrosc.*, 1988, **20**, 207–255.

7 M. Saunders, K. E. Laidig and M. Wolfsberg, *J. Am. Chem. Soc.*, 1989, **111**, 8989–8994.

This journal is © the Owner Societies 2020

Phys. Chem. Chem. Phys., 2020, **22**, 11850–11860 | **11859**

8 P. Vujanić, Z. Meić and D. Vikić-Topić, *Spectrosc. Lett.*, 1995, **28**, 395–405.

9 W. H. Sikorski, A. W. Sanders and H. J. Reich, *Magn. Reson. Chem.*, 1998, **36**, S118–S124.

10 K. Komatsu, M. Murata and Y. Murata, *Science*, 2005, **307**, 238–240.

11 K. Kurotobi and Y. Murata, *Science*, 2011, **333**, 613–616.

12 A. Krachmalnicoff, M. H. Levitt and R. J. Whitby, *Chem. Commun.*, 2014, **50**, 13037–13040.

13 A. Krachmalnicoff, R. Bounds, S. Mamone, S. Alom, M. Concistrè, B. Meier, K. Kouřil, M. E. Light, M. R. Johnson, S. Rols, A. J. Horsewill, A. Shugai, U. Nagel, T. Rõõm, M. Carravetta, M. H. Levitt and R. J. Whitby, *Nat. Chem.*, 2016, **8**, 953–957.

14 S. Bloodworth, G. Sitinova, S. Alom, S. Vidal, G. R. Bacanu, S. J. Elliott, M. E. Light, J. M. Herniman, G. J. Langley, M. H. Levitt and R. J. Whitby, *Angew. Chem., Int. Ed.*, 2019, **58**, 5038–5043.

15 W. I. F. David, R. M. Ibberson, J. C. Matthewman, K. Prassides, T. J. S. Dennis, J. P. Hare, H. W. Kroto, R. Taylor and D. R. M. Walton, *Nature*, 1991, **353**, 147–149.

16 K. Hedberg, L. Hedberg, D. S. Bethune, C. A. Brown, H. C. Dorn, R. D. Johnson and M. D. Vries, *Science*, 1991, **254**, 410–412.

17 C. S. Yannoni, P. P. Bernier, D. S. Bethune, G. Meijer and J. R. Salem, *J. Am. Chem. Soc.*, 1991, **113**, 3190–3192.

18 F. Leclercq, P. Damay, M. Foukani, P. Chieux, M. C. Bellissent-Funel, A. Rassat and C. Fabre, *Phys. Rev. B: Condens. Matter Mater. Phys.*, 1993, **48**, 2748–2758.

19 B. Masenelli, F. Tournus, P. Mélinon, A. Pérez and X. Blase, *J. Chem. Phys.*, 2002, **117**, 10627–10634.

20 S. Díaz-Tendero, F. Martín and M. Alcamí, *Comput. Mater. Sci.*, 2006, **35**, 203–209.

21 M. H. Levitt, *Spin Dynamics. Basics of Nuclear Magnetic Resonance*, Wiley, Chichester, 2nd edn, 2007.

22 F. Cimpoesu, S. Ito, H. Shimotani, H. Takagi and N. Dragoe, *Phys. Chem. Chem. Phys.*, 2011, **13**, 9609–9615.

23 M. Jaszuński, K. Ruud and T. Helgaker, *Mol. Phys.*, 2003, **101**, 1997–2002.

24 L. B. Krivdin and R. H. Contreras, *Annual Reports on NMR Spectroscopy*, Academic Press, 2007, vol. 61, pp. 133–245.

25 M. S. Dresselhaus, G. Dresselhaus and P. C. Eklund, *Science of Fullerenes and Carbon Nanotubes*, Academic Press, New York, 1996.

26 S. Wolfram, *Mathematica: A System for Doing Mathematics by Computer*, Addison-Wesley, New York, 1991.

27 C. Bengs and M. H. Levitt, *Magn. Reson. Chem.*, 2018, **56**, 374–414.

28 P. S. Nielsen, R. S. Hansen and H. J. Jakobsen, *J. Organomet. Chem.*, 1976, **114**, 145–155.

29 J. Jeener, *Advances in Magnetic and Optical Resonance*, Academic Press, 1982, vol. 10, pp. 1–51.

30 M. Mehring, *High Resolution NMR Spectroscopy in Solids*, Springer-Verlag, Berlin Heidelberg, 1976.

31 R. N. Bracewell, *The Fourier Transform and Its Applications*, McGraw Hill, New Delhi, 3rd edn, 2014.